Exp. Theo. NANOTECHNOLOGY 10 (2026) 1633-1654 https://doi.org/10.56053/10.4.1633

Green-synthesized gold nanoparticles from Omani pomegranate peel: Phytochemical characterization and antileishmanial activity

Souad Al Okla[1,], Muna Al-Hinai[2], Chadi Soukkarieh[3], Jamal Al-Sabahi[4], Matthew Gavino Donadu[5,6], Basem Battah[7]*

[1]College of Medicine and Health Sciences, National University of Science and Technology, P.O. Box 391, Sohar 321, Sultanate of Oman
[2]International Maritime College Oman, National University of Science and Technology, P.O. Box 391, Sohar 321, Sultanate of Oman
[3]P.O. Box 30621, Faculty of Science, Damascus University, Damascus, Syria
[4]Central Instrumentation Laboratory, Agriculture College, Sultan Qaboos University, Al-Seeb, Sultanate of Oman
[5]Scuola di Specializzazione in Farmacia Ospedaliera, Department of Medicine, Surgery and Pharmacy, University of Sassari, 07100 Sassari, Italy
[6]Hospital Pharmacy, Giovanni Paolo II Hospital, ASL Gallura, 07026 Olbia, Italy
[7]Department of Biochemistry and Microbiology, Faculty of Pharmacy, Antioch Syrian Private University, Maaret Saidnaya 22734, Syria
*) Email: souadalokla@nu.edu.om

Received 19/5/2026, *Received in revised form* 9/8/2026, *Accepted* 2/9/2026, *Published* 15/10/2026

Omani pomegranate peel is a rich source of phenolic compounds with antioxidant and antimicrobial properties, making it a promising source of antiparasitic bioactive compounds. This study compared air-dried (PPE1) and oven-dried (PPE2) Omani pomegranate peel extracts, chemically synthesized gold nanoparticles (AuNPs), and their green-synthesized AuNP formulations (PPE1–AuNPs and PPE2–AuNPs). Methanolic extracts are prepared from air-dried and oven-dried peels and characterized using UPLC and GC–MS. AuNPs are synthesized using both extracts and characterized by UV–vis spectroscopy and ATR–FTIR. Antileishmanial activity is evaluated against *Leishmania tropica* promastigotes using dose-dependent viability assays. PPE1 exhibited a phytochemical profile characterized by higher

total phenolic content and ellagic acid enrichment (~58% of total phenolics), whereas PPE2 is enriched in chlorogenic acid (~45% of total phenolics) and rutin hydrate, which accounted for approximately 99% of the quantified flavonoid content. UV–Vis and ATR–FTIR analyses confirmed successful AuNP formation and phytochemical-mediated surface functionalization. Both extracts inhibited promastigote viability in a dose-dependent manner, with PPE1 exhibiting greater potency (IC_{50} = 15,200 µg/mL) than PPE2 (IC_{50} = 36,710 µg/mL). Among all tested formulations, chemically synthesized uncoated AuNPs display the greatest antileishmanial activity (IC_{50} = 12.0 µg Au/mL), whereas peel-capped AuNPs are less potent (PPE1–AuNPs: IC_{50} = 71.9 µg Au/mL; PPE2–AuNPs: IC_{50} = 118.2 µg Au/mL). These findings demonstrate the dual role of Omani pomegranate peel phytochemicals as antiparasitic bioactive compounds and as effective reducing and stabilizing agents for environmentally sustainable AuNP synthesis. The results further demonstrate that phytochemical-mediated surface functionalization influences the antileishmanial activity of gold nanoparticles and support the potential of pomegranate-derived nanomaterials for future antiparasitic applications. Further studies should evaluate activity against intracellular amastigotes and determine host-cell selectivity to further assess therapeutic potential.

Keywords: *Leishmania* promastigotes; Pomegranate peel extract; Antileishmanial activity; Gold nanoparticles; Green synthesis

1. INTRODUCTION

Leishmaniasis is a neglected tropical disease caused by protozoan parasites of the genus Leishmania and remains an important public health concern, particularly in low- and middle-income countries [1,2]. Clinically, leishmaniasis manifests as three principal forms: visceral leishmaniasis (VL), cutaneous leishmaniasis (CL), and mucocutaneous leishmaniasis (MCL), with CL representing the most prevalent form [1,2]. According to the World Health Organization (WHO), approximately 700,000–1,000,000 new cases occur annually worldwide, although the true disease burden is likely underestimated because of substantial underreporting in endemic regions [1]. The geographic distribution of CL is highly concentrated, with most reported cases occurring in a limited number of countries in the Eastern Mediterranean Region, the Americas, and parts of Africa and Asia [2]. Cutaneous lesions may also be complicated by secondary bacterial infections, including infections caused by Staphylococcus aureus, whereas HIV coinfection can adversely affect disease presentation, therapeutic response, and recurrence [3,4]. During Leishmania infection, host production of reactive oxygen and nitrogen species contributes to parasite killing; however, excessive generation of these reactive species may also promote oxidative stress and damage to host proteins, lipids, and nucleic acids [5]. Despite advances in diagnosis and disease control, the clinical management of leishmaniasis remains challenging because of the limited number of effective drugs, treatment-related toxicity, prolonged therapeutic regimens, variable species-dependent responses, high costs, and the emergence of drug resistance [3,6]. Current therapeutic options include pentavalent antimonial, amphotericin B formulations, miltefosine, pentamidine, and paromomycin; however, no single regimen is uniformly effective against all clinical forms and Leishmania species [3]. Treatment selection and outcomes are further influenced by the infecting species, lesion number, size and anatomical location, host immune status, comorbidities, and the presence of secondary infection [3]. Moreover, although several vaccine candidates have shown encouraging preclinical or early clinical results, no licensed human vaccine against leishmaniasis is currently available [7]. These limitations have stimulated interest in safer, more affordable

therapeutic agents and in nanotechnology-based approaches capable of improving antileishmanial activity, drug delivery, and biological targeting [8].

Punica granatum L. is widely recognized as one of the richest natural sources of bioactive phytochemicals and has attracted considerable attention because of its diverse nutritional and pharmacological properties [9,10]. Among the different anatomical parts of the fruit, the peel represents the richest source of hydrolysable tannins, ellagitannins, phenolic acids, flavonoids, and related polyphenols with potent antioxidant, antimicrobial, anti-inflammatory, and other pharmacological activities [9]. The phytochemical composition of pomegranate is strongly influenced by cultivar, geographical origin, environmental conditions, and postharvest processing [10]. Fruits cultivated under arid and semi-arid environments generally accumulate higher concentrations of phenolic compounds and antioxidant metabolites in response to environmental stress [10]. Pomegranate cultivars grown in Oman, particularly in the Al Jabal Al Akhdar region, possess distinctive physicochemical characteristics together with a phenolic profile rich in hydrolysable tannins and related antioxidant compounds [11,12]. Consequently, Omani pomegranate peel represents a promising and sustainable source of naturally occurring reducing, stabilizing, and surface-functionalizing phytochemicals for green nanoparticle synthesis.

Although studies specifically investigating pomegranate peel against *Leishmania* spp. remain limited, available evidence indicates that *P. granatum*-derived preparations possess promising antileishmanial activity. In an *in vitro* screening of medicinal plants, *P. granatum* extract inhibited intracellular *Leishmania amazonensis* amastigotes [13]. In a murine model of cutaneous leishmaniasis, oral administration of pomegranate juice reduced lesion development and improved antioxidant enzyme activity in BALB/c mice infected with *Leishmania major* [14]. Collectively, these findings support the continued exploration of pomegranate-derived phytochemicals as promising candidates for the development of novel antileishmanial therapies [13,14].

Nanotechnology has emerged as a promising platform for the development of novel antimicrobial and antiparasitic therapies by enabling the design of nanomaterials with unique physicochemical properties and enhanced biological performance [8]. Among the various nanomaterials investigated, metallic nanoparticles have attracted considerable attention because their small dimensions, high surface-area-to-volume ratio, tuneable surface chemistry, and capacity for surface functionalization facilitate interactions with microbial and parasitic cells [15]. A recent systematic review of metallic nanoparticles for experimental cutaneous leishmaniasis identify reactive oxygen species generation, membrane disruption, interactions with parasite biomolecules, and metal-ion release among the principal mechanisms underlying their antileishmanial activity [15]. In addition, nickel oxide nanoparticles have demonstrated significant inhibitory activity against *Leishmania tropica* in vitro [16], while nanostructured flaxseed-derived fatty acid formulations have also shown promising biological activity against *L. tropica*, further supporting the therapeutic potential of nanotechnology-based interventions for leishmaniasis [17]. Plant-mediated green synthesis has likewise been successfully applied to titanium dioxide nanoparticles with favourable physicochemical characteristics [18], whereas green-synthesized silver nanoparticles have prepared from medicinal plant extracts have demonstrated excellent physicochemical properties together with potent antibacterial activity [19,20]. Collectively, these studies highlight the expanding role of green nanotechnology in developing environmentally sustainable nanomaterials with potential biomedical and antiparasitic applications.

Among metallic nanomaterials, gold nanoparticles (AuNPs) are particularly attractive because of their excellent chemical stability, favourable biocompatibility, versatile surface chemistry, and tuneable optical properties, making them especially suitable for biomedical applications [21,22]. Conventional AuNP synthesis often relies on hazardous reducing agents, toxic stabilizers, and energy-intensive procedures. In contrast, plant-mediated green synthesis provides a more environmentally sustainable approach by exploiting naturally occurring phytochemicals to reduce gold ions while simultaneously stabilizing the resulting nanoparticles [21,22]. Plant-derived metabolites, including polyphenols, flavonoids, tannins, sugars, and proteins, participate in nanoparticle formation and remain associated with the nanoparticle surface as capping and stabilizing agents, thereby influencing particle size, colloidal stability, surface chemistry, and subsequent biological interactions [21,22]. Owing to its high abundance of phenolic constituents, pomegranate peel represents an attractive natural source of reducing and capping agents for the green synthesis of AuNPs.

Postharvest processing, particularly drying, can substantially influence the concentration, stability, and extractability of phenolic constituents, thereby affecting nanoparticle formation and the composition of the phytochemical surface layer. As the phytochemical corona of green-synthesized AuNPs originates from the reducing plant extract, changes in plant phytochemistry may directly affect nanoparticle physicochemical characteristics, stability, surface functionality, and ultimately biological performance [21,22]. Despite increasing interest in plant-mediated AuNP synthesis, the influence of postharvest processing on phytochemical-mediated nanoparticle formation remains poorly understood. In particular, little is known about how drying-induced alterations in the phytochemical profile of Omani pomegranate peel affect nanoparticle surface functionalization, physicochemical characteristics, and the resulting antileishmanial efficacy of green-synthesized AuNPs against *Leishmania tropica*.

Therefore, the present study aims to characterize the phytochemical composition of Omani pomegranate peel extracts prepared using two drying methods, synthesize and characterize green-synthesized AuNPs, and evaluate and compare the antileishmanial activities of the extracts, green-synthesized AuNPs, and uncoated AuNPs against *L. tropica* promastigotes. In addition, the study investigates how drying-induced phytochemical variation influences nanoparticle surface functionalization, physicochemical characteristics, and antileishmanial efficacy.

2. EXPERIMENTAL

2.1 Reagents

The standards of phenolic acids and flavonoids (gallic acid, 3,4-dihydroxy benzoic acid, chlorogenic acid, vanillic acid, caffeic acid, syringic acid, p-coumaric acid, ferulic acid, cinnamic acid, 2-hydroxycinnamic acid, ellagic acid, kaempferol, rutin hydrate, and quercetin) are purchased from Sigma-Aldrich (St. Louis, MO, USA). All standards are prepared as stock solutions at 100 mg/L in methanol and stored at 4 °C in the dark until use. Chromatographic-grade acetic acid, acetonitrile, methanol, dichloromethane (DCM), and hexane (all from Sigma-Aldrich) are used for extraction and chromatographic analysis. Chloroauric acid ($HAuCl_4$, 339.78 g/ mol**;** MilliporeSigma, Burlington, MA, USA) is used as the gold precursor for gold nanoparticles synthesis.

2.2 Pomegranate peel material and drying procedure

The fresh pomegranate fruits are obtained from local farmers in Seeq, Al-Jabal Al-Akhdar, Oman (23.0873° North, 57.6938° East; 2019 m elevation above sea level). Fresh fruits with an average weight of ~800g/ piece are washed manually, and the peels are separated and rinsed with distilled water. The peels are further divided into two portions. One portion is shade-dried at room temperature for 4 days (PP1; air-dried), whereas the second portion is dried in a forced-air oven at 90oC for 22 h (PP2; oven-dried). Oven drying at 90 °C is selected to achieve rapid, reproducible dehydration to constant weight while limiting microbial growth and enzymatic degradation, enabling a controlled comparison with shade air-drying. The dried peels are ground by an electrical mill, sieved through a 425 μm mesh to obtain a uniform powder, and then stored in a cool, dry place until extraction.

2.3 Chemical profiling of pomegranate peel extracts and lipophilic fractions
2.3.1 Preparation of pomegranate peel extracts

Crude extraction is prepared separately for each dried pomegranate peel powder (PP1 and PP2). Peel powder is extracted with methanol at a sample-to-solvent ratio of 3:7 g/ml, sonicated for 1.5 h and filtered using a Büchner funnel. The filtrate is concentrated under reduced pressure at controlled temperature using a rotary evaporator (Büchi R-215). The resulting methanolic extracts (PPE1 and PPE2) are then sterilized using a 0.22 μm membrane filter.

For UPLC analysis, 0.200 g of each dried extract (PPE1 and PPE2) is brought to a final volume of 2 mL using the UPLC mobile phase. For GC–MS lipophilic profiling, the air-dried peel batch (Peel 1) is milled and sieved (425 μm mesh). A 50 g portion of the sieved powder is mixed with 100 mL deionized water, sonicated for 30 min (Grant XUB5), and vacuum-filtered. The aqueous filtrate is then partitioned with either 10 mL hexane or 10 mL dichloromethane (DCM). The resulting organic phases are collected and concentrated to 2 mL using a rotary evaporator (Büchi R-215).

2.3.2 Ultra-performance liquid chromatography (UPLC) analysis

The phenolic acid profiles of both samples are determined using an ultra-performance liquid chromatography system (LC-30AD, Shimadzu, Kyoto, Japan) equipped with an autosampler (SIL-30A, Shimadzu, Kyoto, Japan) for injecting 10 μL of the samples. Separation is carried out using a Tracer Excel 120 ODS column (3 μm particle size, 3 mm I.D., 150 mm length, Teknokroma, Spain) is maintained at 35 ºC with a gradient program employing a two-solvent system (A: 2% acetic acid, B: acetonitrile). The mobile phase consists of solvent A (2% acetic acid in water) and solvent B (acetonitrile), using the following gradient program: initial conditions 98% A; 0–27 min, 82% A; 27–28 min, 70% A; 28–35 min, 56% A; and 35–50 min, 90% A. The flow rate is 0.35 mL/min.

Detection is performed using a diode array detector (SPD-M20A, Shimadzu, Kyoto, Japan) scanning from 190–800 nm, with monitoring at 280 nm to detect phenolic acids. Compounds are identified by comparison of retention times and UV spectra with authenticated reference standards. Quantification is carried out using external calibration curves, and results are expressed as mg/kg of crude extract and mg/kg of dried peel.

2.3.3 Gas chromatography–mass spectrometry (GC–MS) analysis

The concentrated extracts are analyzed by GC–MS using a Shimadzu GC-2010 Plus gas chromatograph coupled to a GC/MS-QP2010 ULTRA mass spectrometer (electron-impact ionization, autotuned EM voltage; Shimadzu, Kyoto, Japan), equipped with an Rtx-5MS capillary column (30 m × 0.25 mm i.d., 0.25 µm film thickness; Restek, Bellefonte, PA, USA; maximum operating temperature 350 °C). High-purity helium (grade 6.0) is used as the carrier gas at a constant flow rate of 1.0 mL/min. The injector temperature is set to 280 °C, the interface (transfer line) to 270 °C, and the ion source to 270 °C. Samples (1 µL) are injected in split mode (5:1). The GC oven temperature program is as follows: initial temperature 42 °C, ramped at 5.5 °C/min to 325 °C, then held for 10 min (total run time 63.3 min). Mass spectra are acquired in full-scan mode over m/z 40–550. Compounds are putatively identified by comparison of spectra with commercial libraries (NIST 2011 v2.3 and Wiley 9th) in combination with retention behavior on the Rtx-5MS column and are reported semi-quantitatively as relative peak area (%). Solvent blanks and duplicate injections are included to assess carryover and analytical reproducibility.

Extraction and chromatographic analyses are repeated independently to confirm analytical reproducibility. Comparable chromatographic profiles, retention times, and major peak distributions are obtained across repeated preparations and analyses. The results presented herein correspond to representative analyses, while quantitative values are reported for comparative interpretation of PPE1 and PPE2.

2.4 Nanoformulation of PPE-based gold nanoparticles
2.4.1 Preparation of chloroauric acid solution

Gold nanoparticles (AuNPs) are synthesized by using chloroauric acid ($HAuCl_4$) as the gold precursor. A 1 mM HAuCl4 stock solution is prepared by dissolving 0.08587 g HAuCl4 (0.25 mmol) in deionized water, yielding a light-yellow solution, which is then adjusted to a final volume of 250 mL. This $HAuCl_4$ solution is used for both chemically synthesized AuNPs and peel-mediated (green) AuNPs.

2.4.2 Chemical synthesis of uncoated gold nanoparticles

Uncoated AuNPs are prepared by citrate reduction of $HAuCl_4$ (Turkevich–Frens). An aqueous $HAuCl_4$ solution (1.0 mM; 100 mL) is brought to gentle reflux under constant stirring in acid-washed glassware. A freshly prepared trisodium citrate solution (38.8 mM) is then added rapidly to a final citrate concentration of 2.5–3.0 mM. The reaction mixture is maintained at reflux for 15–20 min, during which the color changes from pale yellow to ruby red, indicating AuNP formation. The suspension is then removed from heat and cooled to room temperature.

The colloidal AuNPs are purified by centrifugation at 12,000 × g for 10 min (TG16 centrifuge, Yingtai Instrument Co. Ltd., Changsha, China). The supernatant is discarded, and the pellet is resuspended in Milli-Q water. This washing step is repeated three times. The final suspension is passed through a 0.22 µm sterile membrane filter and stored at 4 °C, protected from light.

2.4.3 Green synthesis and purification of PPE-AuNPs

Gold nanoparticles are capped with pomegranate peel extract are synthesized using PPE1 and PPE2 as biological reducing and stabilizing agents. 5 mL of each extract (PPE1 or PPE2) is mixed with 100 mL of 1 mM $HAuCl_4$ in a glass flask and stirred continuously at 25˚C for 4 hours. The appearance of a color changes from light yellow to dark ruby red indicated PPE-AuNP synthesis. The resulting colloids are stored at 4 °C until characterization. Peel-capped AuNPs are purified by centrifugation at 12,000 × g for 1h at 30 °C (TG16 centrifuge, Yingtai Instrument Co. Ltd., Changsha, China). The nanoparticle pellets are collected, resuspended in Milli-Q water, and washed three times by repeated centrifugation (12,000 × g, 10 min) to remove unbound plant material and residual salts.

2.5 Characterization of PPE-AuNPs

The pomegranate extracts (PPE1 and PPE2) as well as the chemically synthesized uncoated AuNPs, and the peel-capped AuNPs (PPE1-AuNP and PPE2-AuNP) are characterized for optical properties and surface chemistry by UV–Vis absorption spectroscopy and attenuated total reflectance Fourier-transform infrared spectroscopy (ATR–FTIR).

2.5.1 UV-vis absorption spectroscopy

Gold nanoparticle formation is confirmed by UV–Vis absorption spectroscopy using a double-beam spectrophotometer (L7, MesuLab, Guangzhou, China). Prior to measurement, samples are diluted in distilled water to obtain a maximum absorbance below 1.5. An aliquot of 3.5 mL of the diluted sample is transferred to a quartz cuvette for spectral acquisition. UV–vis absorption spectra are recorded in the wavelength range of 200–800 nm at a medium scan speed of 10 nm/s to detect the characteristic surface plasmon resonance (SPR) peak associated with gold nanoparticle formation.

2.5.2 ATR-FTIR analysis

ATR–FTIR spectroscopy is used to assess surface functional groups associated with nanoparticle formation and capping. PPE1, PPE2, uncoated AuNPs, PPE1–AuNP, and PPE2–AuNP, are analyzed using a PerkinElmer SpectraOne instrument over the range 4000–400 cm^{-1}. Samples are placed directly onto the ATR crystal, and spectra are collected to compare changes in O–H, C=O/COO^-, and aliphatic C–H vibrations between the native extracts and the corresponding gold nanoparticle formulations.

2.6 Antileishmanial activity against Leishmania tropica promastigotes
2.6.1 Parasite isolation, identification and culture

Clinical isolates of Leishmania tropica are obtained from patients at the Dermatology Hospital of Damascus University, Syria. The isolates are then transported to the laboratory and confirmed as L. tropica by PCR-based typing. Promastigotes are cultured at 26 °C in RPMI-1640 medium supplemented with 10% heat-inactivated fetal bovine serum (FBS; Sigma-Aldrich), 0.5 mM L-glutamine (Sigma-Aldrich), and 100 U/mL penicillin/streptomycin. Parasite growth and morphology are monitored by inverted light microscopy (400×) to ensure actively motile, logarithmic-phase promastigotes prior to antileishmanial testing. For standardization of inoculum density, promastigotes are fixed in 1% formalin and counted using a hemocytometer under bright-field microscopy [81, 82].

2.6.2 Promastigote viability assay (MTT)

The antileishmanial activity of the pomegranate peel extracts and gold nanoparticle formulations is evaluated against *Leishmania tropica* promastigotes using an *in vitro* viability assay adapted from established nanoparticle screening protocols in *Leishmania* spp. [83].

Promastigotes are seeded in sterile 96-well flat-bottom microplates at a density of 1×10^6 cells/well in RPMI-1640 medium. Cells are then exposed to serial dilutions of each test material: PPE1, PPE2, the $HAuCl_4$ precursor solution, chemically synthesized uncoated AuNPs, and peel-capped AuNPs (PPE1–AuNP and PPE2–AuNP). Test suspensions are prepared from sterile stock solutions (100 mg/mL in DMSO) and diluted into culture medium such that the final DMSO concentration in all wells, including vehicle controls, did not exceed 0.1% (v/v). Final assay concentrations correspond to 5%, 12.5%, and 25% (v/v) of the original stock preparations. Untreated parasites (medium only or medium + 0.1% DMSO) serves as negative controls.

Plates are incubated at 26ºC for 24 h. Following incubation, 10 µL of MTT (3-[4,5-dimethylthiazol-2-yl]-2,5-diphenyl tetrazolium bromide) solution (5 mg/mL) is added to each well and incubated for an additional 3 h 35 min at 26ºC. Formazan crystals are then dissolved using MTT solubilization buffer according to the manufacturer's instructions (Sigma-Aldrich). Absorbance is measured at 540 nm using a microplate reader (HumaReader HS, Human GmbH, Wiesbaden, Germany). Viability is calculated as a percentage relative to the untreated control group, with reduced parasite viability indicating increasing antileishmanial activity.

Each concentration is tested in duplicate within the same plate and all experiments are performed in three independent biological replicates (n = 3).

2.6.3 IC_{50} determination and data analysis

Percentage viability values from the MTT assay are used to generate dose–response curves for each treatment. The 50% inhibitory concentration (IC_{50}), defined as the concentration required to reduce promastigote viability by 50%, is determined by nonlinear regression. Data are fitted to a four-parameter logistic (4PL) model with variable slope, which incorporates the minimum response, maximum response, Hill slope, and the inflection point corresponding to 50% inhibition. Curve fitting and IC_{50} estimation are performed using GraphPad Prism (version 10; GraphPad Software, San Diego, CA, USA). IC_{50} values are reported in µg/mL together with 95% confidence intervals (CI). For gold-containing treatments (uncoated AuNPs, PPE–AuNPs, and $HAuCl_4$), IC_{50} values are expressed as µg Au/mL. Model fit quality is assessed using the coefficient of determination (R^2). Each condition is tested in three independent biological experiments (n = 3), and reported values represent the mean of these biological replicates.

3. RESULTS AND DISCUSSION

3.1 Effect of postharvest drying on the phenolic and flavonoid composition of Omani pomegranate peel extracts

Pomegranate peel extracts are prepared using two postharvest drying methods, namely air drying (PPE1) and oven drying (PPE2). Although both drying methods produce comparable extraction yields (54.9% and 56.7% (w/w), respectively), they generate distinct phytochemical profiles, with PPE1 exhibiting a higher total phenolic content (8659.81 mg/kg extract) and PPE2 a markedly higher total flavonoid content (Table 1). These findings indicate that

postharvest drying primarily affects phytochemical composition rather than extraction efficiency, with air drying favoring phenolic preservation and oven drying enhancing flavonoid extractability. Similar effects of drying on the phytochemical composition and biological activity of pomegranate peel have been reported previously, although the magnitude of these changes depends on the drying method, processing conditions, cultivar, geographical origin, and analytical approach [10,20,21]. The total phenolic content observed for PPE1 is comparable to values reported for pomegranate peels processed under optimized drying conditions [20,21]. Collectively, these findings demonstrate that postharvest drying is a major determinant of the phytochemical composition of pomegranate peel and should therefore be considered an important factor when preparing extracts for biomedical and nanotechnological applications.

UPLC-DAD profiling revealed pronounced quantitative differences in the phenolic composition of the two extracts, although the same 11 phenolic acids and three flavonoids are identified in both samples (Tables 1 and 2). These results indicate that drying primarily altered the relative abundance of individual phytochemicals rather than their overall diversity. Although advanced mass spectrometry-based platforms, including UHPLC–QTOF-MS and UPLC–QQQ-MS, provide broader metabolite coverage and greater structural information, UPLC-DAD enabled reliable identification and targeted quantification of the major phenolic constituents and is well suited for comparative phytochemical profiling between the two drying treatments [22].

Table 1 UPLC characterization of phenolic acids in air-dried (PPE1) and oven-dried (PPE2) Omani pomegranate peel extracts.

	Phenolic Acid	**Retention Time (min) PPE1 / PPE2**	**Concentration (mg/kg extract) PPE 1**	**Concentration (mg/kg extract) PPE 2**	**Concentration (mg/kg dry sample) PPE 1**	**Concentration (mg/kg dry sample) PPE 2**
1	Gallic acid	5.505 / 5.374	889.67 (10%)	262.59 (3%)	142.77	47.00
2	3,4-Dihydroxybenzoic acid	10.030 / 9.867	688.81 (8%)	579.22 (7%)	110.54	103.68
3	Chlorogenic acid	17.270 / 17.136	1238.90 (14%)	3646.63 (45%)	198.81	652.74
4	Vanillic acid	18.083 / 17.951	453.58 (5%)	651.30 (8%)	72.79	116.58
5	Caffeic acid	18.722 / 18.569	95.09 (1%)	174.11 (2%)	15.26	31.17
6	Syringic acid	20.027 / 20.027	58.23 (1%)	52.94 (1%)	9.35	9.48
7	p-Coumaric acid	25.108 / 25.062	42.97 (0%)	49.95 (1%)	6.90	8.94
8	Ferulic acid	27.812 / 27.706	177.88 (2%)	117.56 (1%)	28.55	21.04
9	Ellagic acid	29.741 / 29.697	4994.54 (58%)	2609.05 (32%)	801.51	467.02
10	2-Hydroxycinnamic acid	32.706 / 32.400	18.37 (0%)	10.38 (0%)	2.95	1.86
11	Cinnamic acid	36.334 / 36.266	1.75 (0%)	1.22 (0%)	0.28	0.22
	Total		**8659.81**	**8154.95**	**1389.69**	**1459.72**

Ellagic acid is the predominant phenolic constituent in PPE1, accounting for approximately 58% of the total quantified phenolics, whereas chlorogenic acid predominated in PPE2 (45%) (Figure 1A). Together, ellagic, chlorogenic, and gallic acids accounted for more than 80% of the total quantified phenolics in both extracts, indicating that the phytochemical differences between PPE1 and PPE2 are primarily driven by changes in the relative abundance of these three compounds. The concentration of ellagic acid in PPE1 is approximately 1.9-fold higher than that in PPE2, whereas chlorogenic acid is approximately 2.9-fold higher in PPE2. Gallic acid remained one of the major phenolic constituents in both extracts, representing 10% and 3% of the total phenolic content in PPE1 and PPE2, respectively. The predominance of ellagic and gallic acids is consistent with previous reports describing hydrolysable tannins as the principal phenolic constituents of pomegranate peel, although their abundance varies considerably among cultivars and growing environments [9,23]. The greater retention of ellagic acid in PPE1 is most likely attributable to the milder air-drying process, whereas oven drying may have promoted partial degradation of hydrolysable tannins while increasing the relative abundance of chlorogenic acid [20,21]. In addition, the distinctive environmental conditions of the Al Jabal Al Akhdar region, together with cultivar-specific characteristics, may have contributed to the phenolic profile observed in the present study [10–12]. Collectively, these findings indicate that postharvest drying is an important determinant of the phytochemical composition of pomegranate peel and should therefore be considered when preparing extracts for biomedical and nanotechnological applications.

As shown in Table 2 and Figure 1B, oven drying markedly increase the concentration of extractable flavonoids. PPE2 contains more than twice the rutin concentration of PPE1 (788.49 vs. 368.49 mg/kg extract), resulting in a total flavonoid content of 796.95 mg/kg extract compared with 376.79 mg/kg extract in PPE1, whereas quercetin and kaempferol are detected only at trace levels in both extracts.

Table 2 UPLC characterization of flavonoids in air-dried (PPE1) and oven-dried (PPE2) Omani pomegranate peel extracts.

	Flavonoid	Retention Time (min) PPE1 / PPE2	Concentration (mg/kg extract) PPE1	Concentration (mg/kg extract) PPE2	Concentration (mg/kg dry sample) PPE1	Concentration (mg/kg dry sample) PPE2
1	Rutin hydrate	29.238 / 29.169	368.49 (98%)	788.49 (99%)	59.13	141.14
2	Quercetin	36.069 / 36.016	4.89 (1%)	5.93 (1%)	0.78	1.06
3	Kaempferol	38.429 / 38.367	3.41 (1%)	2.53 (0%)	0.55	0.45
	Total		**376.79**	**796.95**	**60.46**	**142.65**

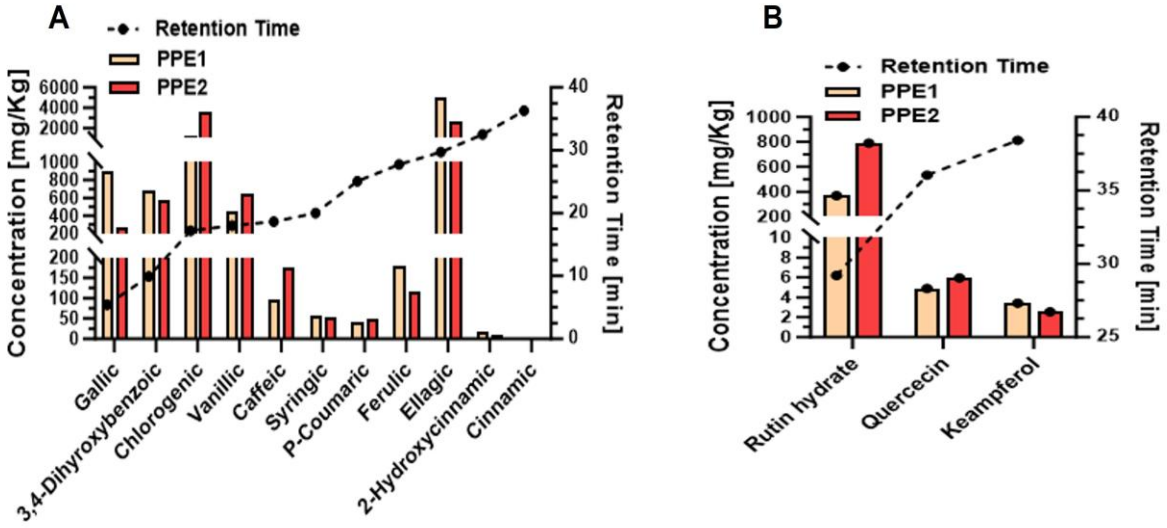

Figure 1 Phenolics and flavonoids in Omani pomegranate peel extracts are determined by UPLC-DAD. Phenolic acids (A) and flavonoids (B) in PPE1 (air-dried) and PPE2 (oven-dried), are reported as concentrations (mg/kg extract); dotted line shows retention time (min).

Rutin accounted for 98–99% of the quantified flavonoids in both extracts, consistent with previous studies identifying it as the predominant flavonoid glycoside in pomegranate peel [9,23]. The substantially higher rutin concentration observed after oven drying suggests that moderate thermal treatment enhanced flavonoid extractability, probably through disruption of the plant cell matrix and improved release of bound flavonoid glycosides, as reported previously for pomegranate peel and other polyphenol-rich plant materials [20,21]. In contrast, quercetin and kaempferol are present only in trace amounts, likely because these flavonoids occur predominantly as glycosylated derivatives, particularly rutin, rather than as free aglycones [9,23]. Despite the greater flavonoid content of PPE2, PPE1 is retained substantially higher concentrations of total phenolics, particularly ellagic acid, highlighting the differential response of hydrolysable tannins and flavonoids to thermal processing. Because phenolic acids and flavonoids differ in antioxidant activity, chemical stability, and biological functions, these compositional differences are likely to influence the overall bioactivity of the extracts. Collectively, these findings establish a biochemical framework for interpreting how drying-induced alterations in phytochemical composition influence the subsequent synthesis, physicochemical characteristics, and biological activity of green-synthesized AuNPs.

3.2 Characterization of lipophilic phytochemicals by GC–MS

To complement the UPLC-DAD characterization of polar phytochemicals, GC–MS analysis is performed on the lipophilic hexane and dichloromethane (DCM) fractions prepared from the air-dried Omani pomegranate peel extract (PPE1). The hexane fraction contained 13 detectable compounds and is dominated by γ-sitosterol (36.08%), followed by 13-octadecenal (16.45%) and cis-oleic acid (12.00%) (Table 3; Figure 2A). Similarly, the DCM fraction contained 14 detectable compounds (11 identified and three unidentified), with γ-sitosterol (25.96%), 13-octadecenal (17.20%), and cis-oleic acid (12.77%) representing the predominant constituents (Table 3; Figure 2B). Despite minor differences in their relative abundance, both solvent fractions exhibited highly comparable lipophilic profiles, indicating that phytosterols and long-

chain fatty acid derivatives constitute the principal non-phenolic constituents of Omani pomegranate peel.

Table 3 GC–MS characterization of major non-phenolic constituents in the hexane and dichloromethane (DCM) fractions of air-dried Omani pomegranate peel (PPE1).

	Compound	Retention Time (min) Hexane / DCM	Relative peak area (%) Hexane	Relative peak area (%) DCM
1	n-Hexadecanoic acid	31.116 / 31.126	2.77	2.60
2	9,12-Octadecadienoic acid (Z,Z)	34.040 / 34.060	2.07	2.47
3	cis-Oleic acid	34.118 / 34.124	12.00	12.77
4	Glycerol 1-palmitate	36.604 / 36.615	8.15	7.27
5	Glycidyl palmitate	36.761 / 36.768	2.49	0.76
6	9,12-Octadecadienal	39.174 / 39.185	5.84	6.46
7	13-Octadecenal, (Z)	39.229 / 39.242	16.45	17.20
8	9,12,15-Octadecatrien-1-ol, (Z,Z,Z)	— / 39.313	—	7.30
9	U.I.	39.955 / 39.400	1.32	1.87
10	U.I.	— / 43.142	—	2.52
11	Pterin-6-carboxylic acid	45.694 / 45.502	2.56	2.32
12	Cholest-5-en-3-ol (3β)-, tetradecanoate	46.872 / —	1.82	—
13	Stigmasta-3,5-diene	47.277 / 47.287	6.89	7.67
14	U.I.	47.719 / 47.727	1.56	2.83
15	γ-sitosterol	49.789 / 49.808	36.08	25.96

Notes: Values are % peak area (semi-quantitative). RT = retention time; DCM = dichloromethane; U.I. = unidentified. Only peaks ≥2.0% in at least one fraction are listed.

The predominance of γ-sitosterol in both fractions is consistent with previous reports describing γ-sitosterol and related phytosterols as characteristic lipophilic constituents of pomegranate peel, although their abundance varies according to cultivar, geographical origin, extraction solvent, and analytical methodology [24–26]. Likewise, the detection of cis-oleic acid, linoleic acid derivatives, glycerol esters, and long-chain aldehydes agrees with previous GC–MS investigations demonstrating that C16–C18 fatty acids and their derivatives represent major lipophilic metabolites of pomegranate peel [24–26]. Collectively, these findings confirm that, in addition to its rich phenolic composition, Omani pomegranate peel contains a chemically diverse lipophilic fraction that may contribute to its biological properties.

Among the identified constituents, γ-sitosterol is of particular interest because phytosterols have been widely reported to possess antioxidant, anti-inflammatory, antimicrobial, and membrane-stabilizing activities that may contribute to the biological properties of plant extracts [27,28]. Although the biological activities of individual lipophilic compounds are not investigated separately in the present study, their coexistence with the abundant phenolic compounds identified by UPLC-DAD suggests that the overall biological activity of PPE1 is

likely the result of complementary interactions among multiple classes of phytochemicals rather than the action of a single dominant metabolite.

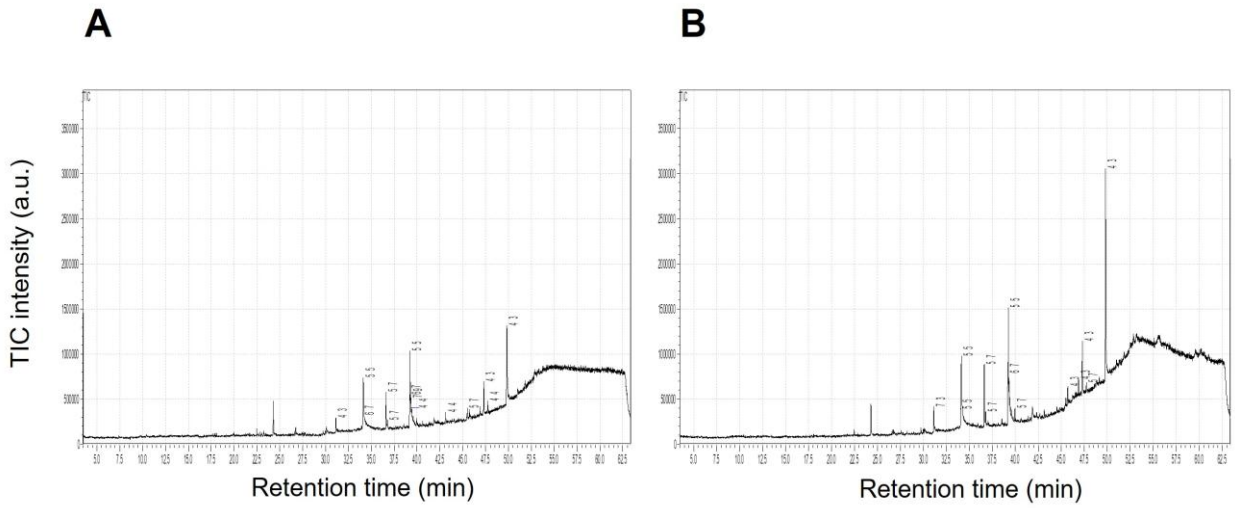

Figure 2 GC–MS total ion chromatograms (TIC) of the lipophilic fractions are obtained from air-dried Omani pomegranate peel (PPE1): (A) hexane fraction and (B) dichloromethane (DCM) fraction. Major peaks correspond to the compounds listed in Table 3.

The GC–MS analysis demonstrates that Omani pomegranate peel contains a diverse array of bioactive lipophilic constituents, particularly phytosterols and long-chain fatty acid derivatives, complementing the phenolic profile identified by UPLC-DAD. This chemically diverse composition further supports the potential of Omani pomegranate peel as a promising botanical source for the green synthesis of AuNPs and their subsequent biological evaluation.

3.3 Green synthesis and physicochemical characterization of gold nanoparticles
3.3.1 UV–vis spectroscopic analysis

The UV–vis spectra of the gold precursor, pomegranate peel extracts, and the synthesized AuNPs are presented in Figure 3. The $HAuCl_4$ precursor (1 mM) exhibits a characteristic absorption band at approximately 310 nm, corresponding to $AuCl_4^-$ ions, and show no absorption in the visible region (Figure 3A). Similarly, the PPE1 and PPE2 extracts display strong absorption in the ultraviolet region attributable to their phenolic constituents but lack any absorption band between 500 and 600 nm, confirming the absence of pre-existing gold nanoparticles (Figure 3B).

Following reaction with $HAuCl_4$, both extracts produce a distinct surface plasmon resonance (SPR) band characteristic of AuNP formation (Figure 3C). PPE1–AuNPs exhibit a sharp, high-intensity SPR peak centered at approximately 555 nm, whereas PPE2–AuNPs display a broader and less intense SPR band extending from approximately 520 to 540 nm.

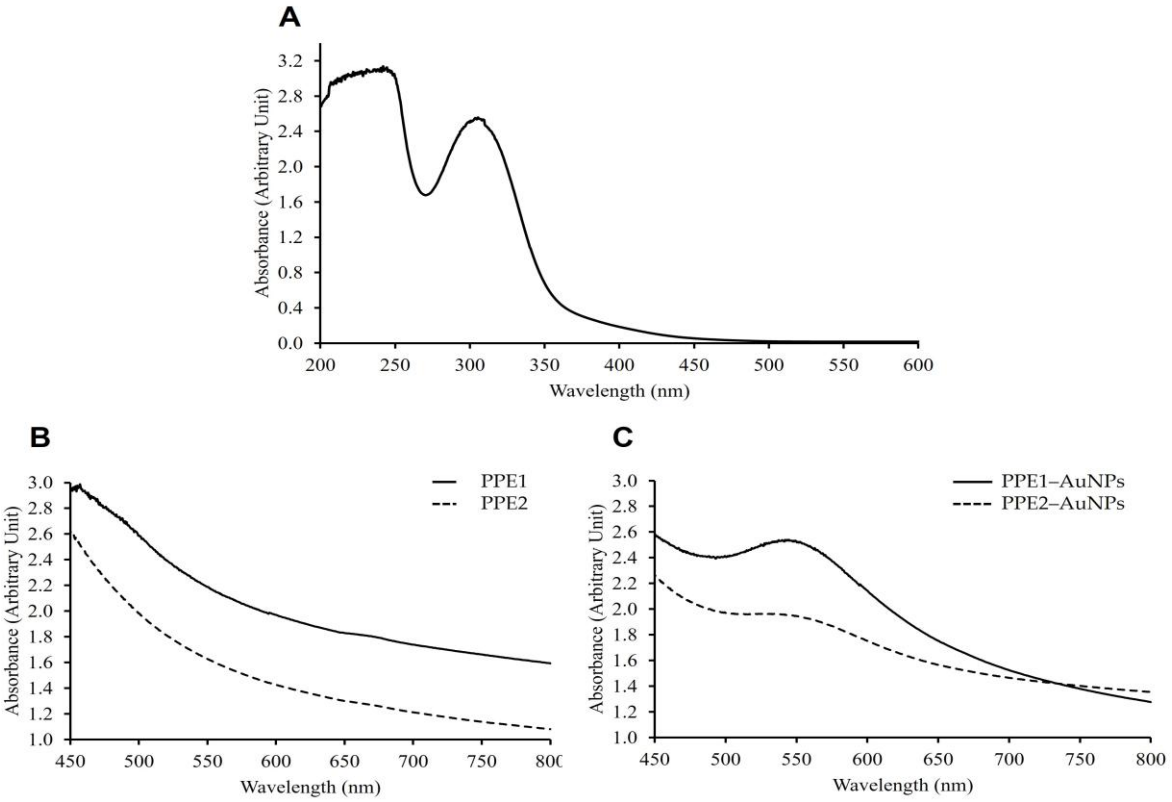

Figure 3 UV–Visible spectra of $HAuCl_4$, pomegranate peel extracts, and green-synthesized AuNPs. (A) Spectrum of 1 mM $HAuCl_4$ showing a characteristic absorption band at approximately 310 nm and no absorption in the visible region. (B) UV–Vis spectra of PPE1 (air-dried) and PPE2 (oven-dried) extracts, exhibiting strong ultraviolet absorption have associated with phenolic compounds but no SPR band. (C) UV–vis spectra of PPE1–AuNPs and PPE2–AuNPs showing characteristic SPR bands of AuNPs, with PPE1–AuNPs exhibiting a sharper, more intense peak ($\lambda max \approx 555$ nm) than PPE2–AuNPs.

The emergence of the characteristic surface plasmon resonance (SPR) band following reaction with $HAuCl_4$ provides clear evidence for the reduction of Au^{3+} ions to metallic Au^0, resulting in the formation of colloidal AuNPs, consistent with previous reports describing plant-mediated synthesis of gold nanoparticles using pomegranate and other polyphenol-rich botanical extracts [21,22,32–34]. The absence of an SPR band in both the precursor solution and the crude extracts further indicates that nanoparticle formation occurred only after the reduction reaction.

The differences have observed in the SPR characteristics of PPE1–AuNPs and PPE2–AuNPs are likely attributable to the distinct phytochemical compositions of the two pomegranate peel extracts. PPE1 has contained substantially higher concentrations of total phenolics, particularly ellagic acid, whereas PPE2 is enriched in flavonoids. Because plant-derived polyphenols act as both reducing and stabilizing agents during green nanoparticle synthesis, variations in their composition can influence nanoparticle nucleation, growth, surface functionalization, and colloidal stability [21,22]. Consequently, the sharper and more intense SPR peak observed for PPE1–AuNPs is consistent with the formation of a more homogeneous nanoparticle population.

The broader SPR band exhibited by PPE2–AuNPs may reflect greater size heterogeneity, aggregation, or differences in surface functionalization arising from the altered phytochemical composition of the oven-dried extract. Similar relationships between SPR band broadening and increased polydispersity or aggregation have been reported for plant-mediated AuNPs synthesized from polyphenol-rich extracts [32–34]. Because both the position and bandwidth of the SPR peak are influenced by nanoparticle size, morphology, aggregation state, and the surrounding dielectric environment, UV–Vis spectroscopy provides only indirect evidence of these characteristics. Therefore, definitive interpretation requires complementary physicochemical characterization to directly evaluate nanoparticle size, morphology, crystallinity, and surface chemistry.

Although UV–Visible spectroscopy provides rapid confirmation of AuNP formation and valuable information regarding the optical properties and dispersion characteristics of AuNPs, it does not permit accurate determination of particle size or morphology. Accordingly, complementary physicochemical characterization is subsequently performed to characterize the structural, morphological, and surface chemical properties of the synthesized AuNPs and to further substantiate the interpretations derived from the UV–vis spectra.

3.3.2 ATR–FTIR spectroscopic analysis

The ATR–FTIR spectra of the pomegranate peel extracts (PPE1 and PPE2) revealed characteristic absorption bands corresponding to the major functional groups present in the phytochemical matrix (Figure 4A). A broad absorption band is centered at approximately 3300 cm^{-1} is assigned to O–H stretching vibrations of phenolic and alcoholic hydroxyl groups, together with aliphatic C–H stretching near 2940 cm^{-1}. Characteristic absorption bands at approximately 1722, 1602, 1330, and 1013 cm^{-1} are attributed to C=O stretching, aromatic C=C stretching, and C–O/C–O–C vibrations associated with phenolic compounds and other oxygenated phytochemicals.

After reaction with $HAuCl_4$, the spectra of both PPE1–AuNPs and PPE2–AuNPs exhibit attenuation and slight shifts of the O–H, C–H, and carbonyl bands, together with the appearance of new bands near 1638 and 1018 cm^{-1} (Figure 4B), indicating the involvement of phytochemicals in both AuNP formation and surface functionalization.

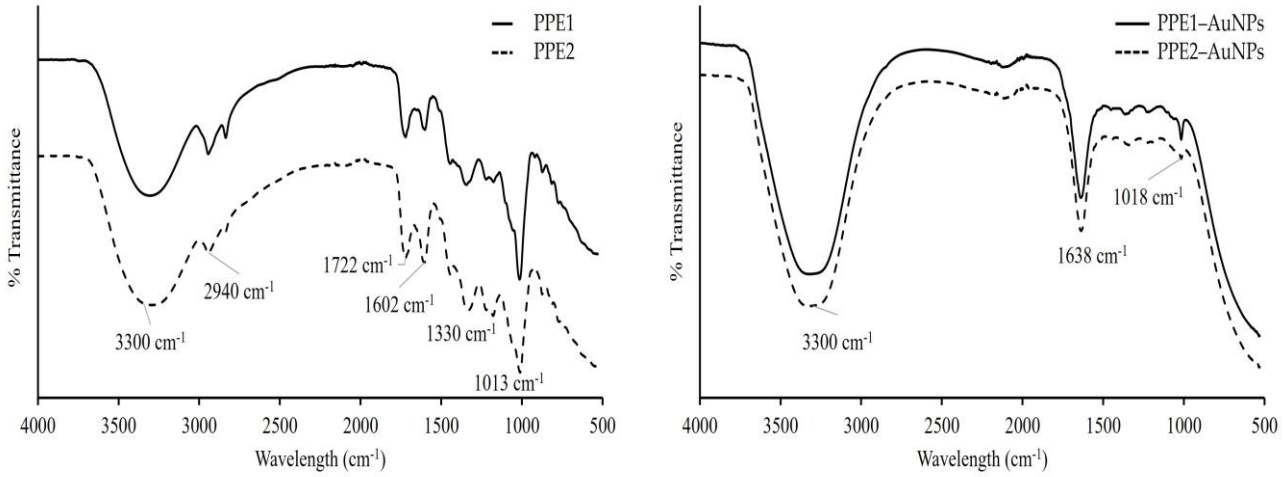

Figure 4 ATR-FTIR spectra of pomegranate peel extracts and the corresponding green-synthesized AuNPs. (A) PPE1 (air-dried) and PPE2 (oven-dried) extracts. (B) PPE1–AuNPs and PPE2–AuNPs are synthesized from the corresponding extracts. Spectra are plotted as % Transmission versus Wavenumber (cm^{-1}).

The attenuation and shifting of the O–H, C=O, and C–O absorption bands indicate the direct involvement of oxygen-containing phytochemicals through their hydroxyl and carboxyl functional groups in the reduction of Au^{3+} ions and stabilization of the resulting AuNPs. These findings are consistent with the UPLC-DAD analysis, which identified ellagic acid, chlorogenic acid, and gallic acid as the predominant phenolic constituents of the extracts. The multiple hydroxyl and carboxyl functional groups present in these compounds facilitate electron transfer to Au^{3+} ions while simultaneously coordinating with the nanoparticle surface, thereby acting as natural reducing, capping, and stabilizing agents [21,22,32].

The appearance of new bands near 1638 and 1018 cm^{-1}, together with the attenuation of hydroxyl and carbonyl vibrations, further supports the formation of a phytochemical corona surrounding the AuNPs. Similar FTIR spectral changes have been consistently reported for plant-mediated AuNPs and are widely recognized as evidence of phytochemical-mediated surface functionalization [33,34].

Although both pomegranate peel extracts successfully produce phytochemical-capped AuNPs, the subtle differences observed in FTIR band intensities suggest that drying-induced variations in phytochemical composition influenced the nature of the surface-bound organic layer. Such differences in surface chemistry are expected to influence nanoparticle stability, surface reactivity, and interactions with parasite membranes, thereby contributing to the differences in antileishmanial activity observed between the two AuNP formulations.

3.4 Antileishmanial activity of pomegranate peel extracts and gold nanoparticles

Dose-dependent viability assays demonstrate that all tested extracts and nanoparticle formulations inhibited the growth of *Leishmania tropica* promastigotes in a concentration-dependent manner (Figure 5A&B). Among the crude extracts, PPE1 exhibited significantly greater antipromastigote activity than PPE2, particularly at 5% and 12.5% (v/v) ($P < 0.0001$; Figure 5C). Consistent with these findings, PPE1 display a substantially lower IC_{50} (15,200

µg/mL; 95% CI: 5,200–24,400; $R^2 = 0.96$) than PPE2 (36,710 µg/mL; 95% CI: 20,900–44,600; $R^2 = 0.99$) (Table 4).

Among the nanoparticle formulations, chemically synthesized uncoated AuNPs exhibited the greatest anti-promastigote activity, with an IC_{50} of 12.0 µg Au/mL (95% CI: 3.0–18.9; $R^2 = 0.99$), followed by $HAuCl_4$ (32.5 µg Au/mL). The green-synthesized formulations retain considerable antileishmanial activity but are less potent, with IC_{50} values of 71.9 µg Au/mL for PPE1–AuNPs and 118.2 µg Au/mL for PPE2–AuNPs (Table 4). These findings demonstrate that chemically synthesized AuNPs exhibit the greatest anti-promastigote activity, whereas PPE2 show the lowest activity. The green-synthesized AuNP formulations display intermediate efficacy, with PPE1–AuNPs consistently outperforming PPE2–AuNPs (Table 4).

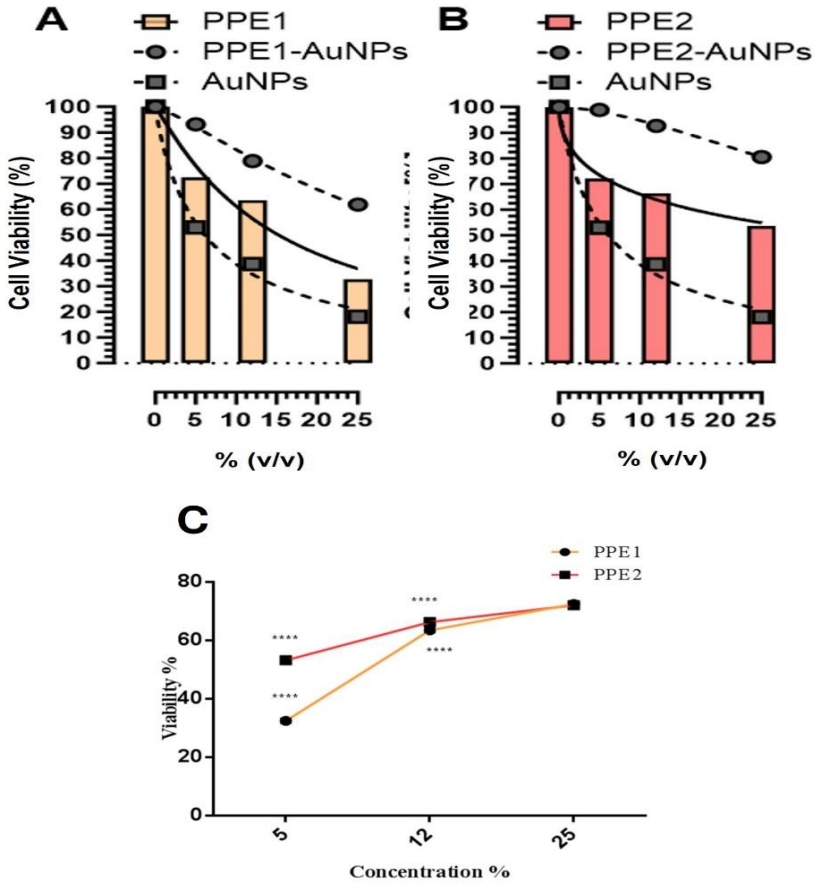

Figure 5 Antileishmanial activity of Omani pomegranate peel extracts and gold nanoparticle formulations against *Leishmania tropica* promastigotes. Dose-dependent inhibition of promastigote viability by (A) PPE1, PPE1–AuNPs, and AuNPs and (B) PPE2, PPE2–AuNPs, and AuNPs. Dose–response curves are fitted using a four-parameter logistic (4PL) model. (C) Comparison of PPE1 and PPE2 at 5, 12.5, and 25% (v/v). Data are presented as mean ± SD. ****P < 0.0001.

Table 4 IC_{50} values of Omani pomegranate peel extracts and gold nanoparticle formulations against *Leishmania tropica* promastigotes.

Treatment	IC_{50} (95% CI)	Goodness of fit (R^2)
PPE1	15,200 µg/mL (5,200–24,400)	0.96
PPE2	36,710 µg/mL (20,900–44,600)	0.99
AuNPs	12.0 µg Au/mL (3.0–18.9)	0.99
$HAuCl_4$	32.5 µg Au/mL (29.3–36.2)	0.99
PPE1–AuNPs	71.9 µg Au/mL (60.1–94.0)	0.99
PPE2–AuNPs	118.2 µg Au/mL (92.4–168.2)	0.99

IC_{50} values are estimated by nonlinear regression using a four-parameter logistic (4PL) model. CI = confidence interval.

The superior anti-promastigote activity of PPE1 is consistent with its phytochemical profile, characterized by substantially higher concentrations of total phenolics, particularly ellagic acid and gallic acid, compared with PPE2. Previous studies have demonstrated significant antileishmanial activity of *Punica granatum* extracts both *in vitro* and *in vivo*, supporting the contribution of its phenolic constituents to the observed biological activity [13,14]. In addition, the GC–MS analysis demonstrated that PPE1 contained abundant phytosterols and long-chain fatty acid derivatives, which possess antioxidant, antimicrobial, and membrane-active properties that may act synergistically with phenolic constituents to enhance anti-promastigote activity [27,28]. Collectively, these findings suggest that preservation of the overall phytochemical composition during air drying is more important for biological activity than increasing the concentration of a single phytochemical class.

Although green synthesis successfully generates biologically active AuNPs, both phytochemical-capped formulations exhibit lower anti-promastigote activity than the chemically synthesized uncoated AuNPs. This observation suggests that nanoparticle surface chemistry plays a critical role in determining biological activity. The UV–Vis and ATR–FTIR analyses demonstrate that phenolic compounds remain associated with the nanoparticle surface following synthesis, forming a phytochemical corona that stabilize the nanoparticles. While this surface functionalization is advantageous for environmentally sustainable synthesis and may improve colloidal stability, it is also likely to partially shield the metallic surface, thereby reducing direct interactions between the nanoparticles and parasite membranes.

Although the precise mechanisms underlying AuNP-mediated parasite killing are not investigated in the present study, previous studies indicate that metallic nanoparticles exert antileishmanial activity through multiple complementary pathways, including disruption of parasite membrane integrity, induction of oxidative stress, mitochondrial dysfunction, and interference with intracellular biomolecules [15,16]. Similar mechanisms have also been proposed for plant-mediated gold nanoparticles, whose biological activity is strongly influenced by nanoparticle size, morphology, and surface chemistry [18,19,29–34]. The substantially greater activity of the uncoated AuNPs observed in the present study is therefore most likely attributable to unrestricted accessibility of the metallic surface, whereas adsorption of phytochemicals onto the nanoparticle surface during green synthesis may partially attenuate these interactions through surface passivation [18,19]. Nevertheless, the phytochemical-coated nanoparticles retain considerable biological activity while offering the advantages of a greener synthesis route that eliminates the need for additional chemical reducing and stabilizing agents.

The present study has several limitations. First, antileishmanial activity is evaluated only against the promastigote stage of *Leishmania tropica*, and the efficacy of the extracts and

nanoparticle formulations against the clinically relevant intracellular amastigote stage remains to be investigated. In addition, host-cell cytotoxicity and selectivity are not assessed, precluding determination of the therapeutic selectivity of the tested formulations. Future studies should therefore include cytotoxicity assessments using relevant mammalian cell lines, particularly macrophages, determine selectivity indices, and evaluate efficacy in intracellular infection models. Furthermore, nanoparticle characterization is limited to UV–Visible spectroscopy and ATR–FTIR analysis. Complementary techniques, including transmission electron microscopy (TEM), X-ray diffraction (XRD), dynamic light scattering (DLS), and zeta potential analysis, would provide more comprehensive information on nanoparticle morphology, crystallinity, particle size distribution, and colloidal stability, thereby strengthening physicochemical characterization and facilitating future biomedical translation.

5. CONCLUSIONS

This study demonstrated that Omani pomegranate peel extracts and both green-synthesized and chemically synthesized gold nanoparticles exhibit antileishmanial activity against *Leishmania tropica* promastigotes, with efficacy influenced by both extract composition and nanoparticle surface chemistry. The air-dried peel extract (PPE1) exhibited greater antipromastigote activity than the oven-dried extract (PPE2), consistent with its higher phenolic content, particularly ellagic acid. Green synthesis of gold nanoparticles using pomegranate peel extracts was successfully achieved, and UV–vis spectroscopy together with ATR–FTIR analyses confirmed nanoparticle formation and phytochemical-mediated surface functionalization. Among all tested formulations, chemically synthesized uncoated AuNPs exhibited the greatest antileishmanial activity, whereas peel-capped AuNPs remained biologically active, demonstrating that phytochemical surface functionalization influences nanoparticle efficacy. These findings demonstrate the dual role of Omani pomegranate peel phytochemicals as antiparasitic bioactive compounds and as effective reducing and stabilizing agents for environmentally sustainable gold nanoparticle synthesis, supporting the potential of pomegranate-derived nanomaterials for future antiparasitic applications. Further studies should evaluate activity against intracellular amastigotes, determine host-cell cytotoxicity and selectivity, and incorporate comprehensive physicochemical characterization to further define the therapeutic potential of these green-synthesized nanoparticle formulations.

References

[1] World Health Organization, Leishmaniasis, World Health Organization, Geneva (2023). https://www.who.int/news-room/fact-sheets/detail/leishmaniasis
[2] World Health Organization, Wkly. Epidemiol. Rec. 99 (2024) 653 https://iris.who.int/handle/10665/379491
[3] H.J.C. de Vries, H.D. Schallig, Am. J. Clin. Dermatol. 23 (2022) 823 https://doi.org/10.1007/s40257-022-00726-8
[4] G.F. Cota, M.R. de Sousa, A.L. de Mendonça, A. Patrocinio, L.S. Assunção, S.R. de Faria, A. Rabello, PLoS Negl. Trop. Dis. 8 (2014) e2816 https://doi.org/10.1371/journal.pntd.0002816
[5] A.C. Costa-da-Silva, D.O. Nascimento, J.R.M. Ferreira, K. Guimarães-Pinto, L. Freire-de-Lima, A. Morrot, D. Decote-Ricardo, A.A. Filardy, C.G. Freire-de-Lima, Trop. Med. Infect. Dis. 7 (2022) 54 https://doi.org/10.3390/tropicalmed7040054
[6] M. Akhoundi, K. Kuhls, A. Cannet, J. Votýpka, P. Marty, P. Delaunay, D. Sereno, PLoS Negl. Trop. Dis. 10 (2016) e0004349 https://doi.org/10.1371/journal.pntd.0004349

[7] I. Saini, J. Joshi, S. Kaur, Cell. Immunol. 399–400 (2024) 104826 https://doi.org/10.1016/j.cellimm.2024.104826
[8] S. Tambe, S. Nag, S.R. Pandya, R. Kumar, K. Balakrishnan, R. Kumar, S. Kumar, P. Amin, P.K. Gupta, ACS Infect. Dis. 10 (2024) 1871 https://doi.org/10.1021/acsinfecdis.4c00010
[9] N. Maphetu, J.O. Unuofin, N.P. Masuku, C. Olisah, S.L. Lebelo, Biomed. Pharmacother. 153 (2022) 113256 https://doi.org/10.1016/j.biopha.2022.113256
[10] A.A. Ghasemi-Soloklui, M. Kordrostami, A. Gharaghani, Sci. Rep. 13 (2023) 15447 https://doi.org/10.1038/s41598-023-42749-z
[11] A.S. Al-Rawahi, Eur. J. Med. Plants 4 (2014) 315–331. https://doi.org/10.9734/EJMP/2014/6417.
[12] F.A. Al-Said, L.U. Opara, R.A. Al-Yahyai, J. Food Eng. 90 (2009) 129 https://doi.org/10.1016/j.jfoodeng.2008.06.012
[13] M. García, L. Monzote, A.M. Montalvo, R. Scull, Pharm. Biol. 48 (2010) 1053–1058. https://doi.org/10.3109/13880200903485729
[14] B. Alkathiri, M.F. El-Khadragy, D.M. Metwally, E.M. Al-Olayan, M.A. Bakhrebah, A.E. Abdel Moneim, Int. J. Environ. Res. Public Health 14 (2017) 1592 https://doi.org/10.3390/ijerph14121592
[15] R.O. Gonçalves, J.R.C. Nascimento, P.E.F. Silva, R.M. Barbosa, T.A.M. Silva, T.S.F. Almeida, P.I.R. Ferreira, C.J.F. Oliveira, J.R. Menezes, L.A.S. Tavares, W.F. Rocha, V.R. Júnior, A.C.A. Santos, M.V. Silva, Parasitol. Res. 123 (2024) 121 https://doi.org/10.1007/s00436-024-08171-3
[16] M.A.M. Al-Doori, N.A. Faris, N.A. Mahmood, A.T. Al-Douri, L.M. Ibrahim, A.M. Al-Tikrity, Exp. Theor. Nanotechnol. 9 (2025) 555 https://doi.org/10.56053/9.4.555
[17] M.A.M. Al-Doori, A.T. Al-Douri, N.A. Faris, Exp. Theor. Nanotechnol. 9 (2025) 489 https://doi.org/10.56053/9.3.489
[18] R.A. Rasheed, M.F.A. Alias, Exp. Theor. Nanotechnol. 10 (2026) 69 https://doi.org/10.56053/10.1.69
[19] A.S. Hussein, Y.W. Younis, S.J.M. Alnajm, S.T. Mahmood, S.A.A. El-Tekreti, M.Q. Mohammed, A.Y. Alwan, A.S. Zaham, A.T. Al-Douri, N.K. Ismael, M.A.M. Al-Doori, Exp. Theor. Nanotechnol. 9 (2025) 505 https://doi.org/10.56053/9.3.505
[20] S.S. Salman, A.T. Al-Douri, A.A. Hadi, S.J.M. Alnajm, Exp. Theor. Nanotechnol. 9 (2025) 361 https://doi.org/10.56053/9.2.361
[21] T. Dinh, Z. Dobó, Á.B. Palotás, H. Kovács, Mater. Today Chem. 48 (2025) 103003 https://doi.org/10.1016/j.mtchem.2025.103003
[22] Z. Fatima, R. Saleem, R.R.M. Khan, M. Liaqat, M.P. Bhatti, Z. Saeed, G. Muhammad, M. Amin, S. Rasheed, Biocatal. Agric. Biotechnol. 59 (2024) 103271 https://doi.org/10.1016/j.bcab.2024.103271
[23] J. Wu, X. Wang, R. Jiang, G. Zhang, Y. Dang, Food Biosci. 64 (2025) 105947 https://doi.org/10.1016/j.fbio.2025.105947
[24] A. Sarkar, M.A. Haque, M. Alam, Food Chem. Adv. 4 (2024) 100622 https://doi.org/10.1016/j.focha.2024.100622
[25] G. Man, L. Xu, Y. Wang, X. Liao, Z. Xu, Front. Nutr. 8 (2022) 807447 https://doi.org/10.3389/fnut.2021.807447
[26] S. Shahkoomahally, D. Shin, F. Habibi, J. Kim, A. Sarkhosh, Food Chem. Adv. 2 (2023) 100225 https://doi.org/10.1016/j.focha.2023.100225
[27] J. Singh, H.P. Kaur, A. Verma, A.S. Chahal, K. Jajoria, P. Rasane, S. Kaur, J. Kaur, M. Gunjal, S. Ercisli, R. Choudhary, M.R. Bozhuyuk, E. Sakar, N. Karatas, M.S. Durul, ACS

Omega 8 (2023) 35452 https://doi.org/10.1021/acsomega.3c02586
[28] F. Azmat, M. Safdar, H. Ahmad, M.R.J. Khan, J. Abid, M.S. Naseer, S. Aggarwal, A. Imran, U. Khalid, S.M. Zahra, F. Islam, Food Sci. Nutr. 12 (2024) 661 https://doi.org/10.1002/fsn3.3777
[29] S.M. Badshah, N. Sultana, M.B.A. Al-Rawi, Z. Tariq, K.S. Lin, A. Hussain, W. Syed, D. Ahmed, J. Hussain, B. Khan, F.U. Rehman, Sci. Rep. 15 (2025) 26689 https://doi.org/10.1038/s41598-025-03596-2
[30] M. Shen, L. Yuan, J. Zhang, X. Wang, M. Zhang, H. Li, Y. Jing, F. Zeng, J. Xie, Foods 13 (2024) 1754 https://doi.org/10.3390/foods13111754
[31] R. Zhang, Y. Han, D.J. McClements, D. Xu, S. Chen, J. Agric. Food Chem. 70 (2022) 2483 https://doi.org/10.1021/acs.jafc.1c07390
[32] S. Niaz, S. Khan, H.N. Khan, I.U. Khan, A.N. Sabri, S. Naseem, S. Riaz, J. Sol-Gel Sci. Technol. 118 (2026) 36 https://doi.org/10.1007/s10971-025-07016-9
[33] S. Bawazeer, A. Rauf, T. Nawaz, A. Khalil, M. Javed, N. Muhammad, M. Shah, Green Process. Synth. 10 (2021) 882 https://doi.org/10.1515/gps-2021-0080
[34] P. Monika, M.N. Chandraprabha, R. Hari Krishna, M. Vittal, C. Likhitha, N. Pooja, V. Chaudhary, C. Manjunatha, Biotechnol. Genet. Eng. Rev. 40 (2024) 3379 https://doi.org/10.1080/02648725.2022.2122299

© 2026 The Authors. Published by LPCMA (https://etnano.com). This article is an open access article distributed under the terms and conditions of the Creative Commons Attribution license (http://creativecommons.org/licenses/by/4.0/).